Theoretical and Applied Fracture Mechanics 104 (2019) 102351

Contents lists available at ScienceDirect

Theoretical and Applied Fracture Mechanics

journal homepage: www.elsevier.com/locate/tafmec

The Bridged Crack Model with multiple fibers: Local instabilities, scale effects, plastic shake-down, and hysteresis

Alberto Carpinteri, Federico Accornero*

Department of Structural, Geotechnical and Building Engineering, Politecnico di Torino, 24 C.so Duca degli Abruzzi, 10129 Torino, Italy

ARTICLE INFO

Keywords:
Fiber-reinforced material
Bridged Crack Model
Snap-back
Snap-through
Plastic shake-down
Hysteresis

ABSTRACT

The Bridged Crack Model is a nonlinear fracture mechanics application, which explains and describes crack propagation phenomena for brittle-matrix fiber-reinforced structural elements in bending. It takes into account the fiber bridging action, which opposes to crack opening and propagation. The flexural response of a fiber-reinforced element is governed by a dimensionless parameter called brittleness number, N_P, which depends on the reinforcement percentage, the fiber yield strength, the matrix fracture toughness, and the element size. In particular, by varying N_P, a ductile-to-brittle transition in the structural response arises. The reinforcement induces some local discontinuities in the moment-rotation diagram, revealing local snap-back and/or snap-through unstable branches.

In the first part of the present work, the application of the Bridged Crack Model to beams reinforced with multiple fibers allows to define a minimum reinforcement criterion, as well as to investigate on the transition from a localized to a continuous reinforcement distribution.

In the second part of the paper, the behaviour of fiber-reinforced cross-sections subjected to cyclic loading is discussed, including phenomena of plastic shake-down and hysteresis. It is demonstrated that the plastic shake-down moment of a single fiber is twice the plastic moment of the same fiber. In particular, for low values of N_P, the plastic shake-down moment is lower than the fracture propagation moment. On the other hand, for high values of N_P, unstable fracture propagation precedes the shake-down, and energy dissipation is not possible.

1. Introduction

Brittle matrix fiber-reinforced materials are characterized by enhanced strength, ductility, and fracture toughness thanks to the bridging action exerted by the fiber reinforcements. The Bridged Crack Model [1–7] allows to clearly explore the mechanical behaviour of fiber-reinforced beams subjected to bending, taking into account the elastic-perfectly brittle matrix, and a rigid-perfectly plastic law of the reinforcements, that can represent either yielding or reinforcement slippage [8,9]. Different versions of this model have been used to describe the microcracking of fiber-reinforced materials as well as macrocracking of materials reinforced by a rather small number of elements [1–4]. In both cases, the Bridged Crack Model is able to explain and reproduce the constitutive flexural response that is often discontinuous owing to the presence of virtual catastrophic branches, i.e., snap-through branches due to load control, and snap-back branches due to deflection control [1–4,10,11]. The bridging tractions are assumed as constant plastic forces, whereas the crack runs in an elastic brittle matrix. The effect of the size scale is considered as fundamental for the global structural behaviour, which can range from ductile to catastrophic simply with the variation of a dimensionless brittleness number, N_P, which is a function of the toughness of the matrix, of the yielding or slippage limit of the reinforcement, of the volume fraction of the reinforcement, and of a characteristic structural size [4,12].

The model described in the present paper considers a fiber-reinforced brittle matrix rectangular cross-section with an edge crack: beam section, initial crack depth, and the position of the fibers are shown in Fig. 1. Only the fibers crossing the crack are considered as active.

It is possible to define a normalized crack depth (Eq. (1)), and a normalized position of the generic fiber reinforcement (Eq. (2)), with respect to the bottom of the beam:

$$\xi = a/b \tag{1}$$

$$\zeta_i = h_i/b \tag{2}$$

The fiber reinforcements exert a bridging action across the crack described by the forces F_i (Fig. 1).

* Corresponding author.
E-mail address: federico.accornero@polito.it (F. Accornero).

https://doi.org/10.1016/j.tafmec.2019.102351
Received 28 May 2019; Received in revised form 1 September 2019; Accepted 11 September 2019
Available online 13 September 2019

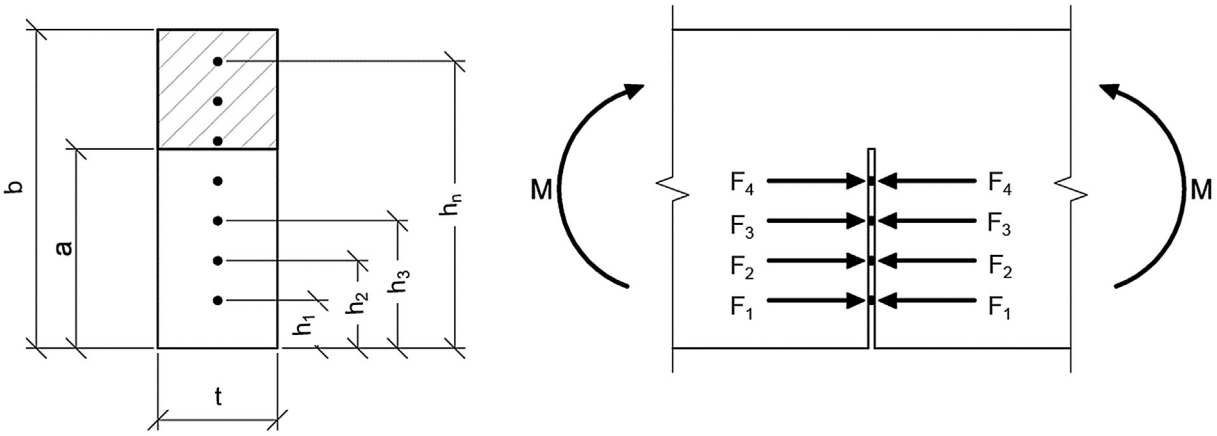

Fig. 1. Fiber-reinforced brittle matrix beam model.

The matrix is assumed to be elastic-perfectly brittle and it is characterized by the fracture toughness, K_{IC}, and the Young Modulus, E, whereas the reinforcements are considered rigid-perfectly plastic, and their ultimate force is equal to $F_{P,i}$. In the slippage hypothesis, the value of $F_{P,i}$ is related to the frictional bonding force between the matrix and the reinforcement, whereas in the hypothesis of yielding, it represents the force that makes the fiber plastically flow. This force is proportional to the area of the reinforcement, A_i and to its yielding stress, $\sigma_{P,i}$. The same value is assumed both in tension and in compression:

$$F_{P,i} = A_i \sigma_{P,i} \tag{3}$$

The Bridged Crack Model takes into account both equilibrium and compatibility equations [13]. The crack opening displacements at the reinforcement levels can be evaluated by using the Superposition Principle: it is necessary to sum two contributions, the first due to the bending moment, and the second due to the concentrated forces, representing the fiber actions applied on the crack faces:

$$w_i = \lambda_{iM} M - \sum_{j=1}^{n} \lambda_{ij} F_j \tag{4}$$

In the previous equation, the minus sign is related to the fact that a positive bending moment tends to open the crack, whereas a traction force tends to close the crack.

The problem is statically indeterminate because the fiber force value is unknown: in order to solve it, the compatibility equations are introduced. Considering the rigid-perfectly plastic law of the fibers, the crack opening displacements at the fiber levels are equal to zero until the ultimate force $F_{P,i}$ is reached [4]. If the bending moment is known, the reactions in the reinforcements, $\{F\}$, can be calculated by solving the linear equation system:

$$[\lambda]\{F\} = \{\lambda_M\} M \tag{5}$$

When the i-th fiber reaches its ultimate force, the crack opening displacement starts increasing. The force transmitted by the fiber becomes known and equal to $F_{P,i}$, whereas the corresponding opening displacement, w_i, remains unknown.

The crack propagation condition is evaluated according to Linear Elastic Fracture Mechanics. The crack propagates when the stress-intensity factor reaches its critical value, K_{IC} [14–18]. Within the Bridged Crack Model, the stress-intensity factor is considered as the sum of two contributions, the first due to the bending moment, and the second due to the reinforcement reactions:

$$K_I = K_{I,M} - \sum_{i=1}^{n} K_{I,i} \tag{6}$$

The minus sign in the previous equation is related to the fact that a positive bending moment tends to open the crack, whereas a positive force closes it [19–20].

It is worth recalling that the flexural response of a fiber-reinforced element is controlled by a dimensionless parameter called brittleness number, N_P, which depends on the reinforcement percentage, the fiber yield strength, the matrix fracture toughness, and the element's size [4]: $N_P = \frac{\sigma_P b^{1/2}}{K_{IC}} \rho$.

2. Monotonically increasing loading

Within the Bridged Crack Model, the behaviour of a fiber-reinforced beam subjected to bending can be evaluated by studying the evolution of the fracturing process, and defining for each crack depth the crack-propagation moment, M_F, and the corresponding localized rotation, φ. The dimensionless crack propagation moment depends on the crack depth, the fiber reactions, the mechanical and geometrical characteristics of the cross-section.

In this way, it is possible to capture the unstable structural behavior which is represented by the negative slope of the moment versus rotation softening branch [10,11,21]. As a matter of fact, in extremely brittle cases, crack propagation occurs suddenly with a catastrophic drop in the load carrying capacity, and the moment versus rotation softening branch assumes a positive slope. If the loading process is controlled by the rotation, the mechanical response presents a discontinuity, and the representative point drops onto the lower branch with negative slope. This means that both moment and rotation must decrease to obtain a controlled crack propagation. Such a phenomenon, the so-called snap-back instability, was deeply investigated with reference to crack growth in elastic-softening materials [11,22,23]. On the other hand, by means of the Bridged Crack Model it is also possible to detect the snap-through instability, that is represented by an horizontal jump at constant load in the moment versus rotation diagram [6].

Snap-back and snap-through phenomena occur during the different phases of cracking in fiber-reinforced structural elements: whereas the cusp catastrophe (snap-back) is basically due to brittle fracturing of the cross-sectional matrix, snap-through is due to plastic deformation of fiber reinforcements.

In Fig. 2 it is possible to observe local snap-back instabilities in the case of a number of fibers $n = 3$, and a brittleness number $N_P = 0.8$. Snap-back instabilities manifest by the vertical drops A-A', B-B', and C-C'.

In Fig. 3, local snap-through instabilities are shown in the case of loading control. Snap-through instabilities manifest by the horizontal jumps A-A', B-B', and C-C'.

In Fig. 4, dimensionless moment versus rotation curves are shown, obtained by varying the brittleness number, N_P, from 0.1 to 1.0, for a beam cross-section with one single layer of reinforcement ($n = 1$)

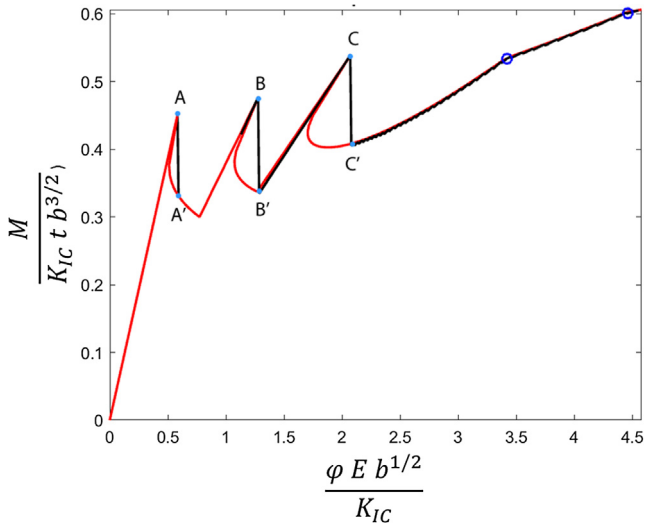

Fig. 2. Dimensionless moment versus rotation for a cracked beam subjected to bending: Snap-back instabilities. The red curve is obtained by means of the Crack Length Control Scheme, while the black one represents the rotation control. Blue circles indicate the yielding of the fibers. (For interpretation of the references to colour in this figure legend, the reader is referred to the web version of this article.)

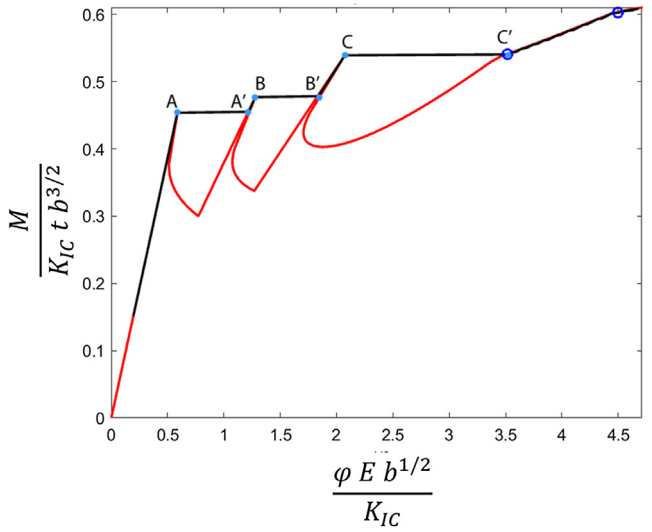

Fig. 3. Dimensionless moment versus rotation for a cracked beam subjected to bending: Snap-through instabilities. The red curve is obtained by means of the Crack Length Control Scheme, while the black one represents the loading control. Blue circles indicate the yielding of the fibers. (For interpretation of the references to colour in this figure legend, the reader is referred to the web version of this article.)

positioned in $h = 0.1b$, and with a notch depth equal to the cover. Notice how different structural behaviours are predicted by the Bridged Crack Model by varying N_P, which represents a synthetic parameter governing the structure ultimate response. By analysing the different behaviours shown in Fig. 4, a ductile-to-brittle transition can be determined according to which, from a strain-softening structural response for low N_P values, a strain-hardening one appears for high N_P values. In brief, for a cross-section with $n = 1$, a critical value of the brittleness number, N_{PC}, which represents the ductile-to-brittle transition, is found to be equal to 0.55, allowing to define a minimum reinforcement ratio [24] identified by the dashed line in Fig. 4.

The curves obtained for $N_P < N_{PC}$ are characterized by softening branches, which can be experimentally observed only if the loading process is controlled by a displacement parameter, in order to prevent unstable crack propagation.

In Figs. 5 to 9, dimensionless moment versus rotation curves are shown by varying the brittleness number, N_P, from 0.1 to 1.0, for a beam cross-section with a number of fibers, n, equal to 2, 3, 5, 10, respectively, and with an initial crack depth corresponding to the cover. As previously shown, snap-back and snap-through phenomena occur, respectively, during brittle fracturing of the cross-sectional matrix, and plastic deformation of fiber reinforcements. It is worth noting that the critical brittleness number, N_{PC}, varies starting from 0.67 for $n = 2$ (dotted line).

In Fig. 10, ductile-to-brittle transitions represented by the critical values of the brittleness number, N_{PC}, are calculated for a beam cross-section with a number of reinforcement layers, n, varying from 1 to 160. We obtain the asymptotical value $N_{PC} = 1.30$, which can be considered as the condition of minimum reinforcement for $n \to \infty$, i.e., for a continuous distribution of fibers.

Furthermore, from Fig. 10 it can be deduced that the condition of distributed continuous reinforcements into the matrix can be simulated through $n > 20$, allowing the Bridged Crack discrete model to be very effective in multi-fiber brittle matrix composites analysis. The limit case, $n = 20$, characterises the starting point of the asymptotic branch, representing the sufficiently large number of reinforcement layers which allows the continuous and discontinuous formulations to converge to the same global results [6].

3. Cyclic loading

The Bridged Crack Model with multiple fibers above presented in the case of monotonic loading, can be extended to the case of cyclic loading [8,25,26], since it is possible to divide a generic load history in different phases, each one characterized by an increase or a decrease in load, as shown in Fig. 11.

Eq. (5), in addition to a compatibility equation, can be rewritten in incremental form by subtracting the initial condition (subscript 0) from the current value:

$$\{w\} - \{w_0\} = \{\lambda_M\}(M - M_0) - [\lambda](\{F\} - \{F_0\}) \tag{7}$$

$$\{w\} - \{w_0\} = \{0\} \tag{8}$$

Eq. (8) is valid only for fiber reinforcements in the elastic condition. On the other hand, considering a generic situation with both elastic (subscript c) and plastic (subscript f) fibers, it is possible to split the problem into a statically indeterminate and a statically determinate part:

$$\begin{Bmatrix} w_f \\ w_c \end{Bmatrix} - \begin{Bmatrix} w_{0,f} \\ w_{0,c} \end{Bmatrix} = \begin{Bmatrix} \lambda_{Mf} \\ \lambda_{Mc} \end{Bmatrix}(M - M_0) - \begin{bmatrix} \lambda_{ff} & \lambda_{fc} \\ \lambda_{cf} & \lambda_{cc} \end{bmatrix}\left(\begin{Bmatrix} F_f \\ F_c \end{Bmatrix} - \begin{Bmatrix} F_{0,f} \\ F_{0,c} \end{Bmatrix}\right) \tag{9}$$

with the conditions $F_{f,i} = \pm F_{P,f,i}$, and $\{w_c\} = \{w_{0,c}\}$. The sign $\pm$ depends on the direction of loading: the positive value is related to the loading phase, whereas the negative one attains to the unloading phase.

The rotation can be computed as:

$$\varphi - \varphi_0 = \lambda_{MM}(M - M_0) - \sum_{j=1}^{m} \lambda_{jM}(F_j - F_{0,j}) = \lambda_{MM}(M - M_0) - \{\lambda_M\}^T (\{F\} - \{F_0\}) \tag{10}$$

Also in the case of cyclic loading, the numerical results can be effectively represented in a moment vs. rotation diagram. If the crack propagation does not occur, three different stages characterize the system response shown in Fig. 12 ($n = 2$):

1. Linear elastic: $M < M_{P,1}$
2. Linear hardening and elastic shake-down: $M_{P,1} < M < M_{SD,1}$
3. Plastic shake-down: $M > M_{SD,1}$

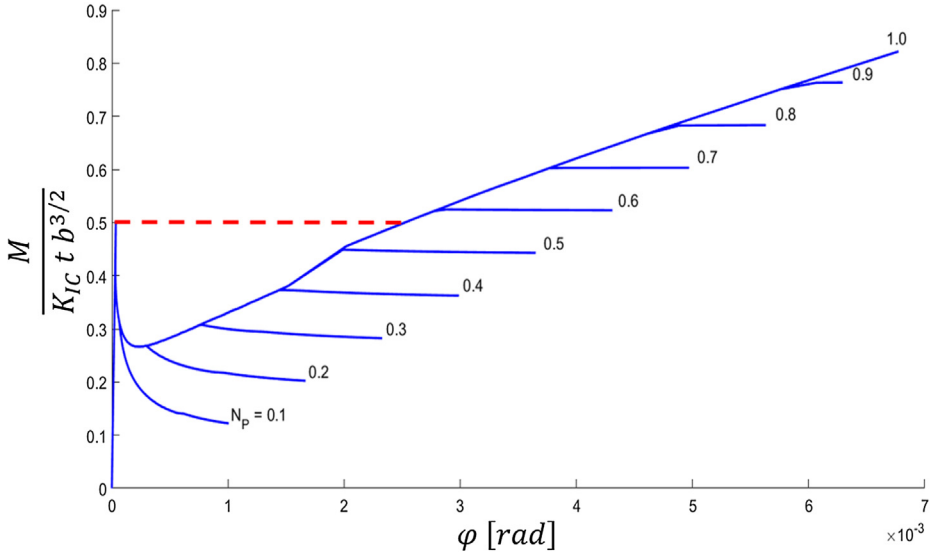

Fig. 4. One single fiber abacus (beam cross-section with $n = 1$).

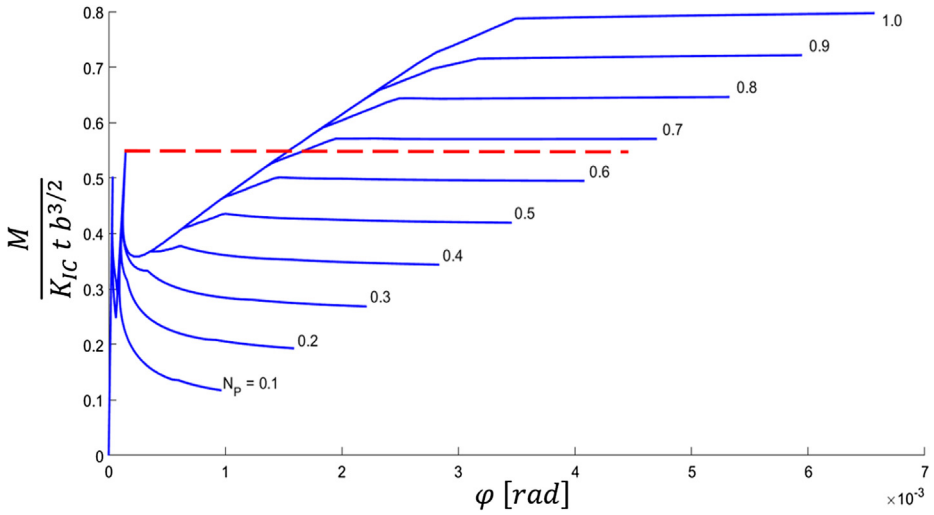

Fig. 5. Two-fibers abacus (beam cross-section with $n = 2$).

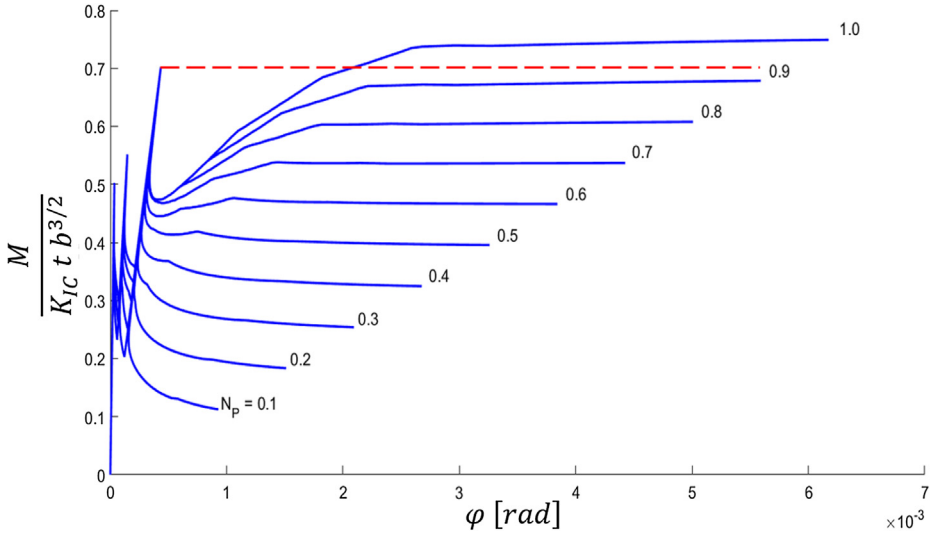

Fig. 6. Three-fibers abacus (beam cross-section with $n = 3$).

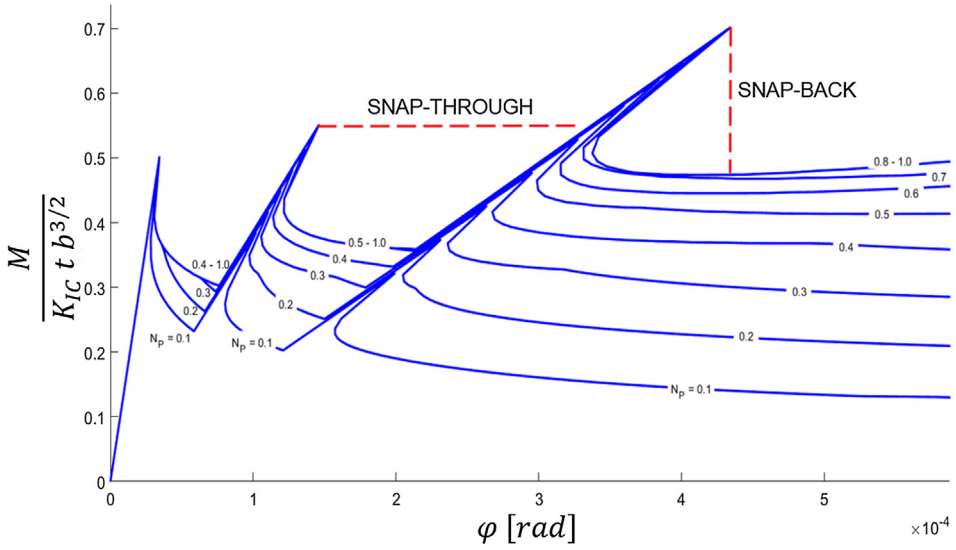

Fig. 7. Three-fibers abacus (Zoom): Snap-through and snap-back instabilities.

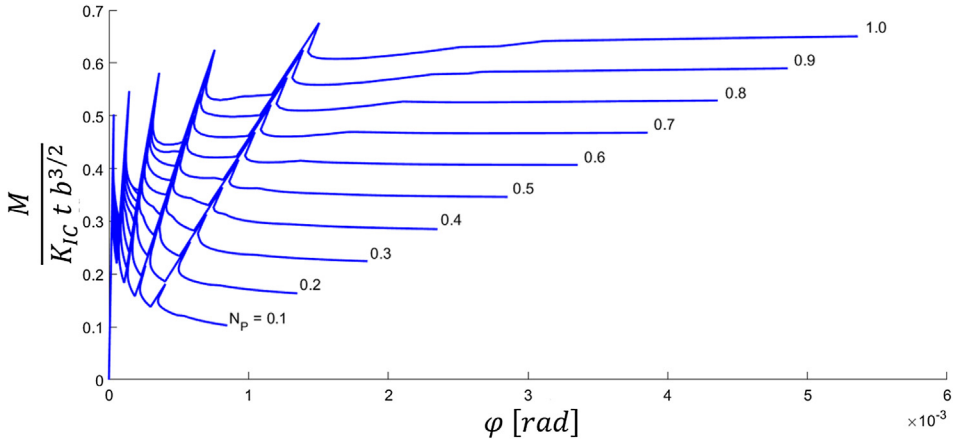

Fig. 8. Five-fibers abacus (beam cross-section with $n = 5$).

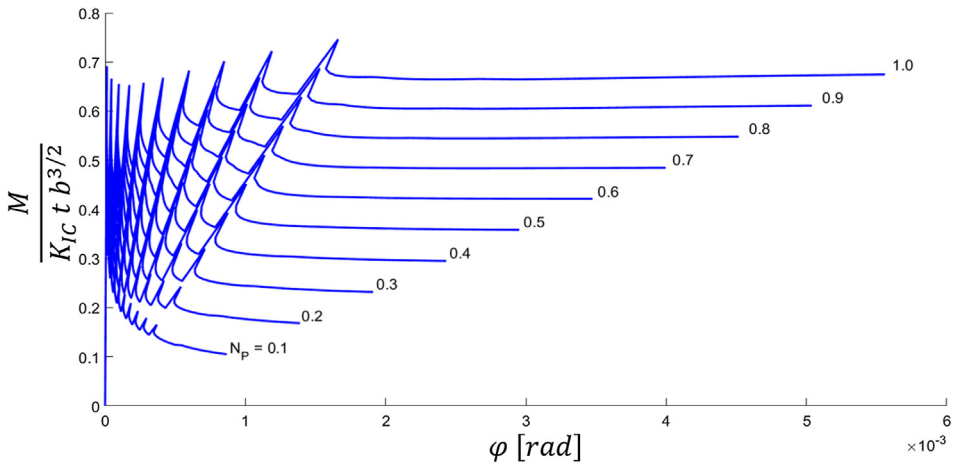

Fig. 9. Ten-fibers abacus (beam cross-section with $n = 10$).

As it is shown in Fig. 12, the fiber undergoes yielding in compression only when the corresponding shake-down moment is overcome, due to the hysteretic cycle between $M_{SD,1}$ and $M_{SD,2}$. If the shake-down moment is not reached, the unloading phase occurs on a single elastic branch without hysteretic cycle, energy dissipation, and compression yielding.

In order to define the plastic moment values, the fiber reactions are calculated from Eq. (5):

$$F_i = [\lambda]_i^{-1}\{\lambda_M\}M \tag{11}$$

where i indicates the i-th row of the matrix $[\lambda]^{-1}$.

Then, the condition $F_i = F_{P,i}$ is considered, and the corresponding

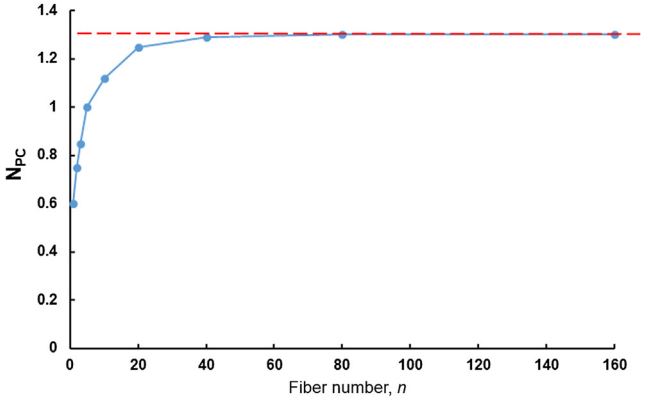

Fig. 10. Critical value of the brittleness number, N_{PC}, versus fiber number, n, for the Bridged Crack discrete model ($h_1/b = 0.1$).

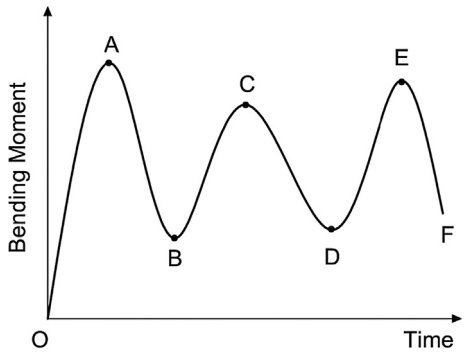

Fig. 11. Decomposition of the load history into monotonic phases.

bending moment is evaluated:

$$M_{P,i} = \frac{F_{P,i}}{[\lambda]_i^{-1}\{\lambda_M\}} \tag{12}$$

In the following stage when, at least, one fiber is yielded, we have:

$$\{F_c\} = [\lambda_{cc}]^{-1}[\{\lambda_{Mc}\}M - [\lambda_{cf}]\{F_{P,f}\}] \tag{13}$$

$$F_i = [\lambda_{cc}]_i^{-1}[\{\lambda_{Mc}\}M - [\lambda_{cf}]\{F_{P,f}\}] \tag{14}$$

Again, the condition $F_i = F_{P,i}$ is considered, and the corresponding bending moment is evaluated:

$$F_{P,i} = [\lambda_{cc}]_i^{-1}[\{\lambda_{Mc}\}M_{P,i} - [\lambda_{cf}]\{F_{P,f}\}] \tag{15}$$

$$M_{P,i} = \frac{F_{P,i} + [\lambda_{cc}]_i^{-1}[\lambda_{cf}]\{F_{P,f}\}}{[\lambda_{cc}]_i^{-1}\{\lambda_{Mc}\}} \tag{16}$$

So, the j-th plastic moment is given by:

$$M_{P,j} = \min_{i=1,n_c} \frac{F_{P,i} + [\lambda_{cc}]_i^{-1}[\lambda_{cf}]\{F_{P,f}\}}{[\lambda_{cc}]_i^{-1}\{\lambda_{Mc}\}} j = 2, \cdots, n \tag{17}$$

Moreover, it can be shown that the shake-down moment, M_{SD}, of a generic fiber is always twice the relative plastic moment, M_P. The fiber reactions can be calculated as:

$$\{F_c\} - \{F_{0,c}\} = [\lambda_{cc}]^{-1}[\{\lambda_{Mc}\}(M - M_0) - [\lambda_{cf}](\{F_f\} - \{F_{0,f}\})] \tag{18}$$

$$F_i - F_{0,i} = [\lambda_{cc}]_i^{-1}[\{\lambda_{Mc}\}(M - M_0) - [\lambda_{cf}](\{F_f\} - \{F_{0,f}\})] \tag{19}$$

The conditions $F_i = -F_{P,i}$, $F_{0,i} = F_{P,i}$, $M = 0$, $M_0 = M_{SD,i}$, $\{F_f\} = -\{F_{P,f}\}$ and $\{F_{0,f}\} = \{F_{P,f}\}$ are considered, and the corresponding bending moment is evaluated, proving that:

$$-F_{P,i} - F_{P,i} = [\lambda_{cc}]_i^{-1}[\{\lambda_{Mc}\}(-M_{SD,i}) - [\lambda_{cf}](-\{F_{P,f}\} - \{F_{P,f}\})] \tag{20}$$

$$M_{SD,i} = \frac{2(F_{P,i} + [\lambda_{cc}]_i^{-1}[\lambda_{cf}]\{F_{P,f}\})}{[\lambda_{cc}]_i^{-1}\{\lambda_{Mc}\}} \tag{21}$$

The j-th shake-down moment is the minimum of Eq.(21), and it is twice the j-th plastic moment of Eq.(17).

In the following, size effects are examined [27], in addition to the influence of the fiber number and the crack depth on the hysteresis phenomenon.

Generally speaking, the increase in the brittleness number, N_P, involves an increase in the hysteretic cycle area, its shape remaining unchanged. As a matter of fact, if N_P doubles, the plastic and shake-down moments double too, and consequently the dissipated energy value becomes four times larger. This behaviour is depicted in Fig. 13, in which three different values of N_P are considered. The energy dissipation increase is related to the value of the last shake-down moment.

On the other hand, in Fig. 14 it is possible to notice that an increase in the crack depth, ξ, entails a decrease in plastic and shake-down moments, the deformation becoming larger and larger. At the same time, the area of the hysteretic cycle (dissipated energy) decreases.

The effect of the fiber number, n, is illustrated in Fig. 15. In this case

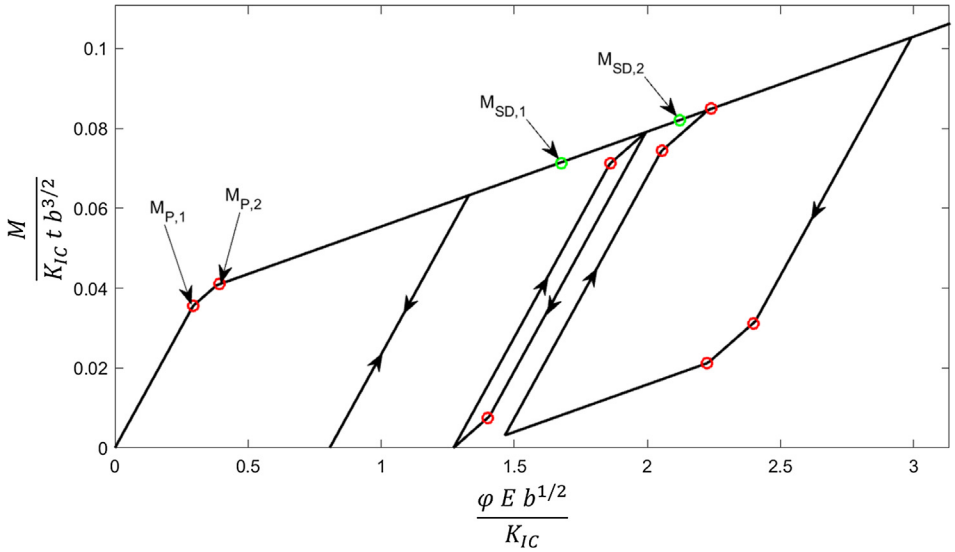

Fig. 12. Shake-down and hysteresis for a cross-section with $n = 2$. Red circles indicate the yielding of the fibers, while green ones represent plastic shake-down moments. (For interpretation of the references to colour in this figure legend, the reader is referred to the web version of this article.)

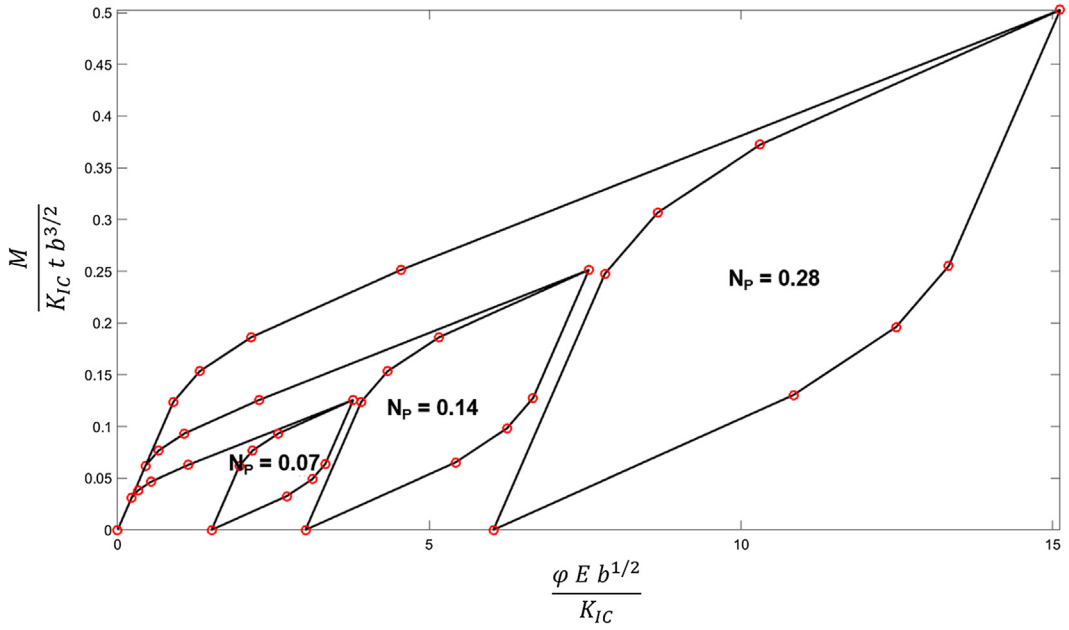

Fig. 13. Influence of N_P for a cross-section with $n = 4$. Red circles indicate the yielding of the fibers. (For interpretation of the references to colour in this figure legend, the reader is referred to the web version of this article.)

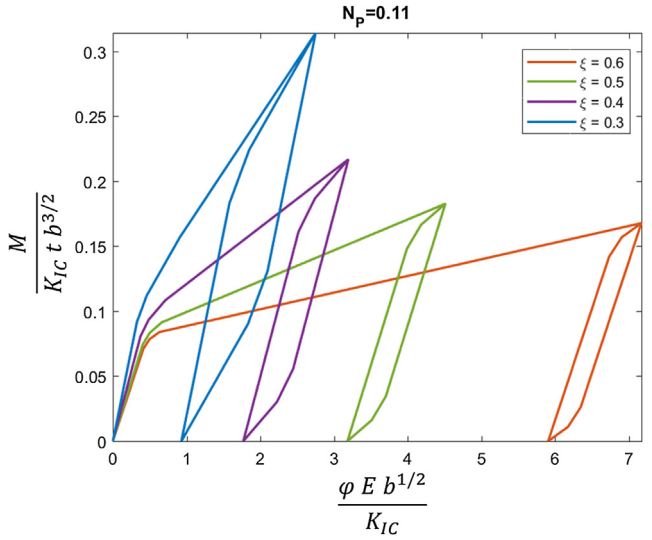

Fig. 14. Influence of ξ for a cross-section with $n = 3$.

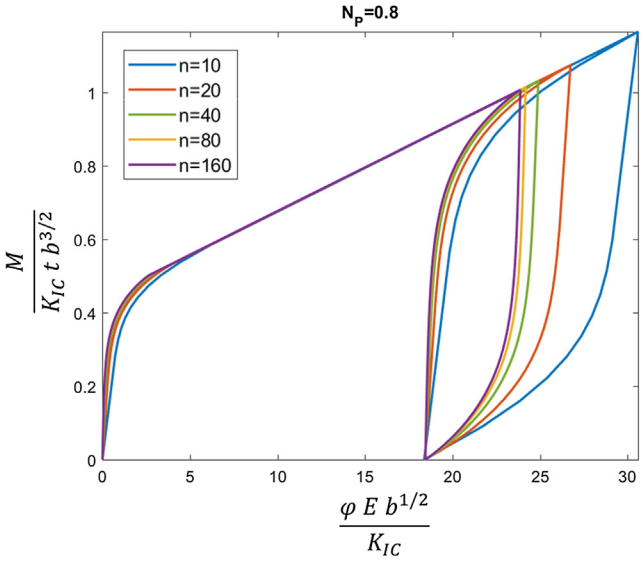

Fig. 15. Influence of fiber number, n, for a cross-section with constant reinforcement percentage. The maximum load is related to the plastic shake-down.

the brittleness number, N_P, and the total reinforcement percentage are taken as constants, whereas n is increased from 10 to 160. It is possible to notice that, increasing n, the value of the shake-down moment decreases. For large n values, the hysteretic cycles tend to the same shape, and the values of the shake-down moment converge.

In Fig. 16, the cases with $n = 10$ and $n = 80$ are compared for the same maximum load, highlighting the influence of n on the hysteresis. The dissipated energy related to the curve with $n = 80$ is about 20% larger than the one obtained for $n = 10$. Consequently, in a fiber-reinforced cross-section, keeping the total reinforcement percentage as constant, a fiber number increase leads to a more dissipative behaviour of the structural system.

If both brittleness number, N_P, and fiber number, n, vary, significant scale effects arise in terms of shake-down and hysteresis.

First of all, a cross-section with three different values of N_P, and $n = 3$ is analysed.

The moment-rotation responses for the three cases are characterised by remarkable local instabilities, as displayed in Figs. 17, 18, and 19.

In Fig. 17, for $N_P = 0.4$, a global strain-softening behaviour is shown, highlighting how low brittleness numbers produce low plastic and shake-down moments. A large hysteretic cycle is found.

In Fig. 18, for $N_P = 0.7$, the ductile-to-brittle transition is emphasized, confirming the minimum reinforcement condition with $n = 3$. In this case, the area of hysteresis is smaller than the area obtained in the previous example ($N_P = 0.4$), but the plastic moment values (blue circles) are larger than in the previous case.

In the last case (Fig. 19), for $N_P = 1.0$, the structural behaviour is strain-hardening, and the hysteretic cycle almost vanishes.

In a similar way, a cross-section with three different values of N_P, and $n = 10$ is now analysed. The moment-rotation responses for the three cases are displayed in Figs. 20, 21, and 22.

In the first case (Fig. 20), for $N_P = 0.4$, a global strain-softening behaviour is shown, in spite of local snap-back instabilities. Eight

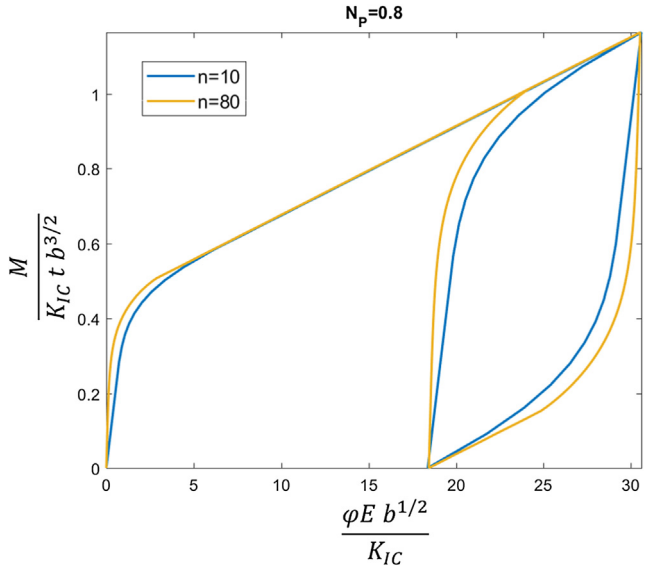

Fig. 16. Influence of the fiber number, n, for a cross-section with constant reinforcement percentage and constant maximum load.

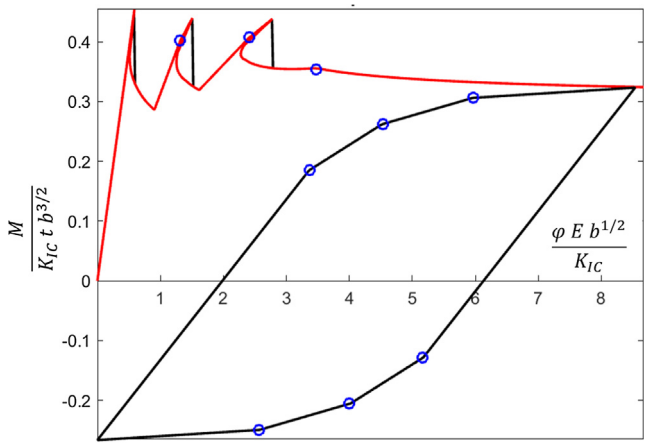

Fig. 17. Moment versus rotation diagram for $N_P = 0.4$, and $n = 3$. The red curve is obtained by means of the Crack Length Control Scheme, while the black one represents the rotation control. Blue circles indicate the yielding of the fibers. (For interpretation of the references to colour in this figure legend, the reader is referred to the web version of this article.)

reinforcements, over ten, reach their compression limit, producing a large hysteretic cycle.

In the second case (Fig. 21), for $N_P = 0.7$, only seven reinforcements, over ten, attain the compression limit, due to the high shake-down moment values.

For $N_P = 1.0$, only five fibers achieve the compression limit, as shown in Fig. 22.

The comparison between the three cases with $n = 10$ is shown in Fig. 23, remarking that, keeping the crack depth constant, the area of the hysteretic cycle (dissipated energy) increases with the increase in the brittleness number.

In addition, comparing the cases of $n = 3$ (Figs. 17–19) with the cases of $n = 10$ (Figs. 20–22), a more dissipative structural behaviour is found for higher values of n.

Finally, it is possible to represent, for constant values of N_P and ξ, the decrease in the shake-down moment as the fiber number increases (Fig. 24), identifying an horizontal asymptote for $n > 80$.

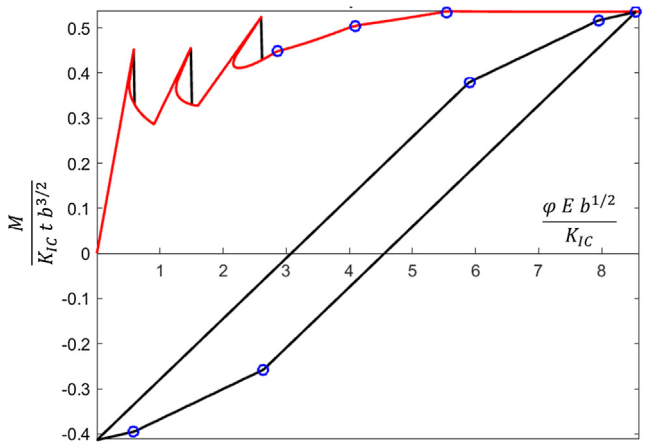

Fig. 18. Moment versus rotation diagram for $N_P = 0.7$, and $n = 3$. The red curve is obtained by means of the Crack Length Control Scheme, while the black one represents the rotation control. Blue circles indicate the yielding of the fibers. (For interpretation of the references to colour in this figure legend, the reader is referred to the web version of this article.)

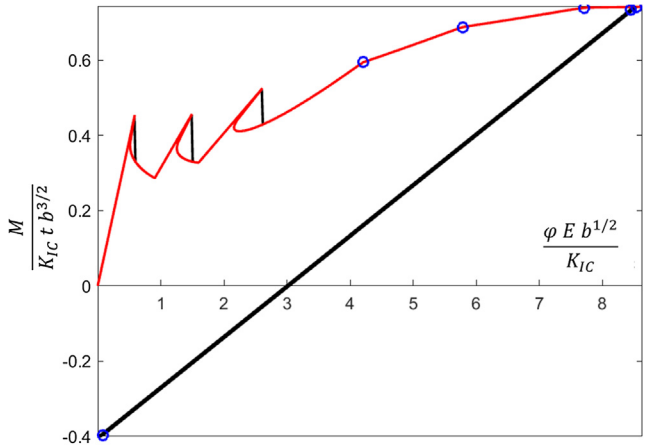

Fig. 19. Moment versus rotation diagram for $N_P = 1.0$, and $n = 3$. The red curve is obtained by means of the Crack Length Control Scheme, while the black one represents the rotation control. Blue circles indicate the yielding of the fibers. (For interpretation of the references to colour in this figure legend, the reader is referred to the web version of this article.)

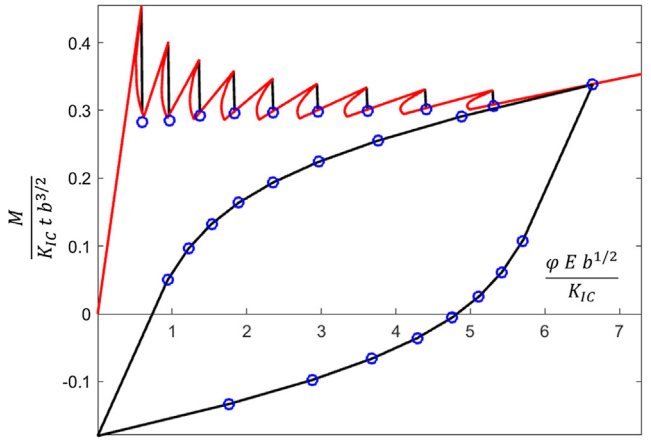

Fig. 20. Moment versus rotation diagram for $N_P = 0.4$, and $n = 10$. The red curve is obtained by means of the Crack Length Control Scheme, while the black one represents the rotation control. Blue circles indicate the yielding of the fibers. (For interpretation of the references to colour in this figure legend, the reader is referred to the web version of this article.)

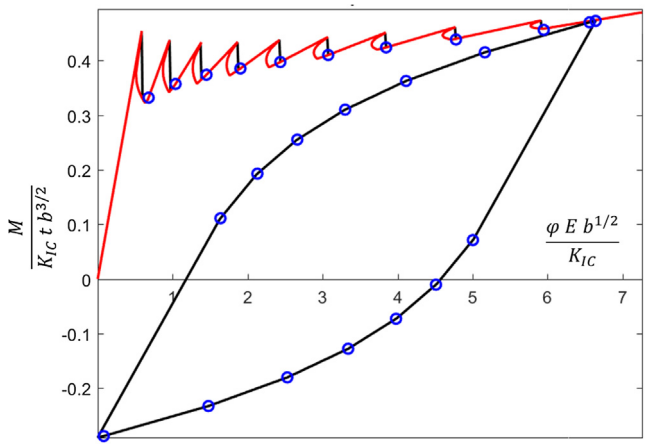

Fig. 21. Moment versus rotation diagram for $N_P = 0.7$, and $n = 10$. The red curve is obtained by means of the Crack Length Control Scheme, while the black one represents the rotation control. Blue circles indicate the yielding of the fibers. (For interpretation of the references to colour in this figure legend, the reader is referred to the web version of this article.)

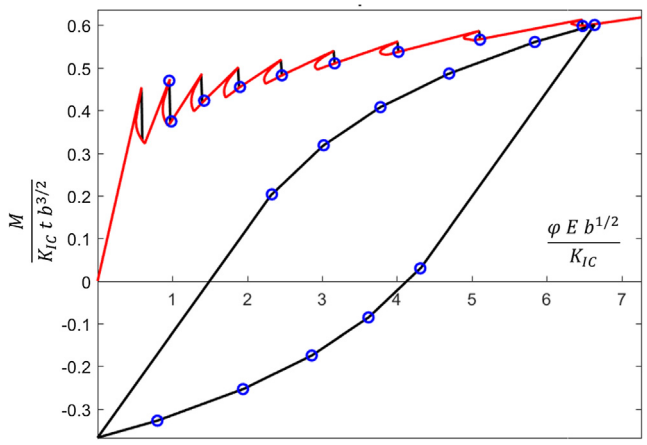

Fig. 22. Moment versus rotation diagram for $N_P = 1.0$, and $n = 10$. The red curve is obtained by means of the Crack Length Control Scheme, while the black one represents the rotation control. Blue circles indicate the yielding of the fibers. (For interpretation of the references to colour in this figure legend, the reader is referred to the web version of this article.)

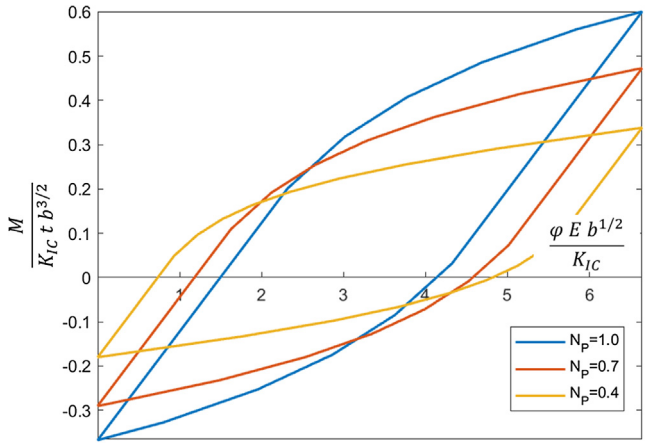

Fig. 23. Dissipated energies for $n = 10$.

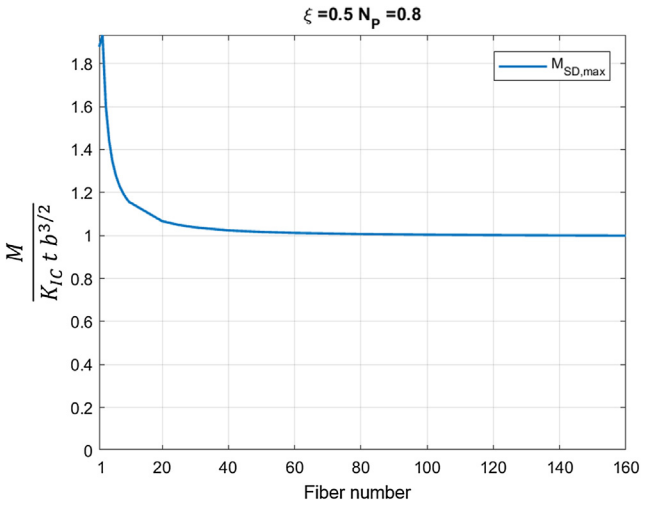

Fig. 24. Shake-down moment versus fiber number for $N_P = 0.8$, and $\xi = 0.5$.

4. Conclusions

In the first part of the present paper, the application of the Bridged Crack Model to brittle-matrix fiber-reinforced structural elements allows to define a minimum reinforcement criterion for cross-sections with multiple layers of reinforcement, investigating the flexural response in the transition from a localized to a continuous reinforcement distribution. In particular, it can be deduced that the condition of distributed continuous reinforcements into the matrix can be simulated through a number of fibers $n > 20$, allowing the Bridged Crack discrete model to be very effective in multi-fiber brittle matrix composites analysis. The limit case, $n = 20$, represents the sufficiently large number of reinforcement layers which allows the continuous and discontinuous formulations to converge to the same global results.

In the second part of this analysis, the behaviour of a fiber-reinforced cross-section subjected to cyclic loading is discussed, with the phenomena of hysteresis and plastic shake-down, highlighting how the shake-down moment related to a fiber is always twice the plastic moment. Moreover, size effects are examined, showing that, in general, an increase in the brittleness number, N_P, involves an increase in the dissipated energy, the hysteretic cycle shape remaining unchanged. On the other hand, in a fiber-reinforced cross-section, keeping the total reinforcement percentage constant, an increase in the fiber number leads to a more dissipative behaviour of the structural system.

Acknowledgments

The authors gratefully acknowledge the effective support of their students Giulio Baffa Giusa and Riccardo Miosi.

References

[1] C. Bosco, A. Carpinteri, P.G. Debernardi, Fracture of reinforced concrete: Scale effects and snap-back instability, Eng. Fract. Mech. 35 (1990) 665–677.
[2] C. Bosco, A. Carpinteri, Fracture behavior of beam cracked across reinforcement, Theor. Appl. Fract. Mech. 17 (1992) 61–68.
[3] C. Bosco, A. Carpinteri, Discontinuous constitutive response of brittle matrix fibrous composites, J. Mech. Phys. Solids 43 (1995) 261–274.
[4] A. Carpinteri, Stability of fracturing process in RC beams, J. Struct. Eng. (ASCE) 110 (1984) 544–558.
[5] A. Carpinteri, R. Massabò, Bridged versus cohesive crack in the flexural behavior of brittle-matrix composites, Int. J. Fract. 81 (1996) 125–145.
[6] A. Carpinteri, R. Massabò, Continuous vs discontinuous bridged crack model of fiber-reinforced materials in flexure, Int. J. Solids Struct. 34 (1997) 2321–2338.
[7] A. Carpinteri, R. Massabò, Reversal in failure scaling transition of fibrous composites, J. Eng Mech. (ASCE) 123 (1997) 107–114.
[8] G.L. Agrawal, L.G. Tulin, K.H. Gerstle, Response of doubly reinforced concrete beams to cyclic loading, ACI J. 62 (1965) 823–834.
[9] K. Visalvanich, A.E. Naaman, Fracture model for fiber reinforced concrete, ACI J. 80

(1983) 128–138.
[10] A. Carpinteri, Cusp catastrophe interpretation of fracture instability, J. Mech. Phys. Solids 37 (1989) 567–582.
[11] A. Carpinteri, F. Accornero, Multiple snap-back instabilities in progressive micro-cracking coalescence, Eng. Fract. Mech. 187 (2018) 272–281.
[12] A. Carpinteri, Size effects on strength, toughness, and ductility, J. Eng. Mech. (ASCE) 115 (1989) 1375–1392.
[13] M.H. Aliabadi, D.P. Rooke, Numerical fracture mechanics, Springer, 1991.
[14] D.J. Cartwright, D.P. Rooke, Approximate stress intensity factors compounded from known solutions, Eng. Fract. Mech. 6 (3) (1974) 563–571.
[15] D.J. Cartwright, D.P. Rooke, Evaluation of stress intensity factors, J. Strain Anal. Eng. Des. 10 (4) (1975) 217–224.
[16] D.P. Rooke, D.J. Cartwright, Compendium of stress intensity factors, Her Majesty's Stationery Office, London, 1976.
[17] D.P. Rooke, F.I. Baratta, D.J. Cartwright, Simple methods of determining stress intensity factors, Eng. Fract. Mech. 14 (2) (1981) 397–426.
[18] E.E. Gdoutos, Fracture mechanics, Springer, 2005.
[19] F. Accornero, G. Lacidogna, A. Carpinteri, Medieval arch bridges in the Lanzo Valleys, Italy: Incremental structural analysis and fracturing benefit, J. Bridge Eng. ASCE 23 (7) (2018) 05018005.
[20] G. Lacidogna, F. Accornero, Elastic, plastic, fracture analysis of masonry arches: A multi-span bridge case study, Curved and Layered Structures 5 (2018) 1–9.
[21] A. Carpinteri, G. Colombo, Numerical analysis of catastrophic softening behaviour (snap-back instability), Comput. Struct. 31 (1989) 607–636.
[22] Lacidogna, G., Accornero, F., Corrado, M., Carpinteri, A., 2013. Crushing and fracture energies in concrete specimens monitored by Acoustic Emission, Proceedings of the 8th International Conference on Fracture Mechanics of Concrete and Concrete Structures, FraMCoS 2013, 1726-1736.
[23] G. Lacidogna, F. Accornero, A. Carpinteri, Influence of snap-back instabilities on Acoustic Emission damage monitoring, Eng. Fract. Mech. 210 (2019) 3–12.
[24] A. Carpinteri, M. Corrado, M. Paggi, G. Mancini, New model for the analysis of size-scale effects on the ductility of reinforced concrete elements in bending, J. Eng. Mech. (ASCE) 135 (2009) 221–229.
[25] A. Carpinteri, An Carpinteri, Hysteretic behavior of RC beams, J. Struct. Eng. (ASCE) 110 (1984) 2073–2084.
[26] A. Carpinteri, S. Puzzi, The bridged crack model for the analysis of brittle matrix fibrous composites under repeated bending loading, J. Appl. Mech. 74 (2007) 1239–1246.
[27] A. Carpinteri, F. Accornero, Rotation versus curvature fractal scaling in bending failure, Phys. Mesomech. 22 (2019) 46–51.